10-16-2008

Middle Miocene Tectonic Boundary Conditions for Use in Climate Models

Nicholas Herold
University of Sydney

M. Seton
University of Sydney

R. D. Müller

Y. You
University of Sydney

Matthew Huber
Purdue University, mhuber@purdue.edu

Geochemistry Geophysics Geosystems G3
AN ELECTRONIC JOURNAL OF THE EARTH SCIENCES
Published by AGU and the Geochemical Society

Article
Volume 9, Number 10
16 October 2008
Q10009, doi:10.1029/2008GC002046
ISSN: 1525-2027

Middle Miocene tectonic boundary conditions for use in climate models

N. Herold, M. Seton, and R. D. Müller
EarthByte Group, School of Geosciences, University of Sydney, Madsen Building F09, Sydney, New South Wales 2006, Australia (nicholas.herold@usyd.edu.au)

Y. You
EarthByte Group, School of Geosciences, University of Sydney, Madsen Building F09, Sydney, New South Wales 2006, Australia

Institute of Marine Science, University of Sydney, Madsen Building F09, Sydney, New South Wales 2006, Australia

M. Huber
Earth and Atmospheric Sciences, Purdue University, West Lafayette, Indiana 47906, USA

[1] Utilizing general circulation models (GCMs) for paleoclimate study requires the construction of appropriate model boundary conditions. We present a middle Miocene paleotopographic and paleobathymetric reconstruction geographically constrained at 15 Ma for use in GCMs. Paleotopography and paleogeography are reconstructed using a published global plate rotation model and published geological data. Paleobathymetry is reconstructed through application of an age-depth relationship to a middle Miocene global digital isochron map, followed by the overlay of reconstructed sediment thickness and large igneous provinces. Adjustments are subsequently made to ensure our reconstruction may be utilized in GCMs.

Components: 5456 words, 6 figures, 2 tables.

Keywords: paleotopography; paleobathymetry; general circulation models.

Index Terms: 1622 Global Change: Earth system modeling (1225); 8157 Tectonophysics: Plate motions: past (3040); 3040 Marine Geology and Geophysics: Plate tectonics (8150, 8155, 8157, 8158).

Received 4 April 2008; **Revised** 15 July 2008; **Accepted** 13 August 2008; **Published** 16 October 2008.

Herold, N., M. Seton, R. D. Müller, Y. You, and M. Huber (2008), Middle Miocene tectonic boundary conditions for use in climate models, *Geochem. Geophys. Geosyst.*, *9*, Q10009, doi:10.1029/2008GC002046.

1. Introduction

[2] An essential step in adapting general circulation models (GCMs) to the study of paleoclimate is the construction of appropriate boundary conditions. The boundary conditions required are typically model- and study-dependent however will necessarily include a global reconstruction of paleogeography, paleotopography, and paleobathymetry.

[3] The growth of the paleoclimate modeling community has led to the need for establishing consistent boundary conditions across research groups in order to facilitate interstudy comparisons and reduce the amount of time spent on data manipula-

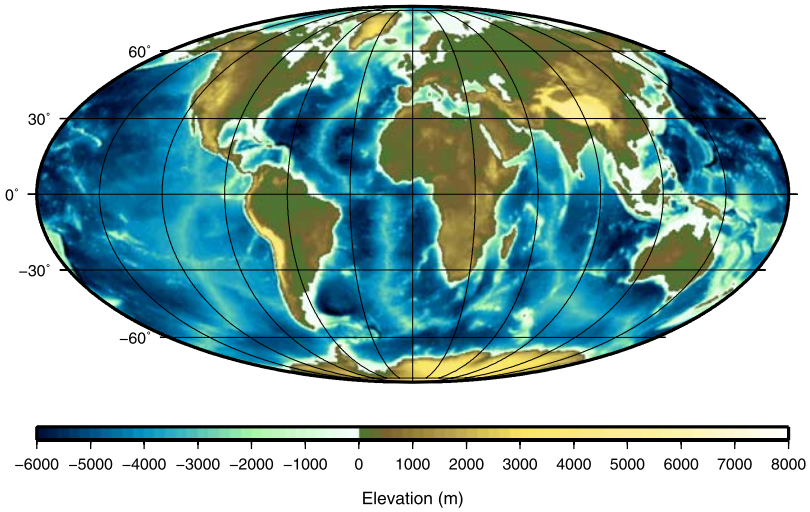

Figure 1. Mollweide projection of present topography and bathymetry using ETOPO2.

tion [e.g., *Sewall et al.*, 2007]. Here we present a global reconstruction of paleotopography and paleobathymetry geographically constrained at 15 Ma (the middle Miocene), and describe the method through which it was developed. Following others [*Markwick*, 2007; *Sewall et al.*, 2007], it is our intent that this reconstruction provide a common boundary condition among research groups modeling middle Miocene climate, and is available from the authors in the various forms presented in this paper.

2. Methods

2.1. Paleogeographic and Paleotopographic Reconstruction

[4] Our middle Miocene paleogeography is based on an underlying plate kinematic model [*Müller et al.*, 2008a, 2008b], which quantitatively describes the relative motions between tectonic plates in a moving Indian/Atlantic hot spot reference frame [*O'Neill et al.*, 2005]. The moving hot spot reference frame accounts for motion between hot spots, producing an improved measure of fit between paleomagnetic data and the locations of hot spots and hot spot trails. This is in contrast to the fixed hot spot reference frame [e.g., *Müller et al.*, 1993] used extensively in previous reconstructions. Additionally, previous studies have obtained paleogeographic data by digitising shorelines from existing paleogeographic maps, primarily using the PALEOMAP project [e.g., *Bice et al.*, 2000; *Sewall et al.*, 2007], or by using unpublished rotations to reconstruct the continents at a particular time with little explanation on how the rotation model was derived [e.g., *Markwick and Valdes*, 2004]. The details of our rotation model are described by *Müller et al.* [2008a, 2008b] and include a table of all plate rotations enabling examination and replication of our geographic reconstructions.

[5] Using our global rotation and plate model, we isolate and subsequently rotate individual continents, continental blocks and island arcs from a present-day digital elevation model (based on ETOPO2; Figure 1) to their position at 15 Ma. Boundaries between continental and oceanic crust are based on the outlines of *Müller et al.* [2008b] and are interpreted from marine geophysical data including ship track magnetic and aeromagnetic data; ship track gravity and gravity anomalies from satellite altimetry [*Sandwell and Smith*, 1997]; ship track bathymetry, ETOPO2, and GEBCO bathymetry data; and seismic reflection data. The outlines of the island arcs are determined from gravity and bathymetry data only.

[6] 2Modifications to the paleogeography and paleotopography are applied to areas where published geological data indicate substantial differences between the middle Miocene and the present (see section 3). The paleotopography is merged with our reconstructed paleobathymetry (see section 2.2) to form a global topographic and bathymetric grid constrained at 15 Ma (Figure 2). Owing to the large computing expense imposed by coupled atmosphere-ocean GCMs and the limited ability to validate high resolution pre-Quaternary climate simulations, such models have often been limited to coarse horizontal resolutions of greater than $3° \times 3°$. For implementation into GCMs and to aid our model required adjustments (see section 2.3), our reconstruction is

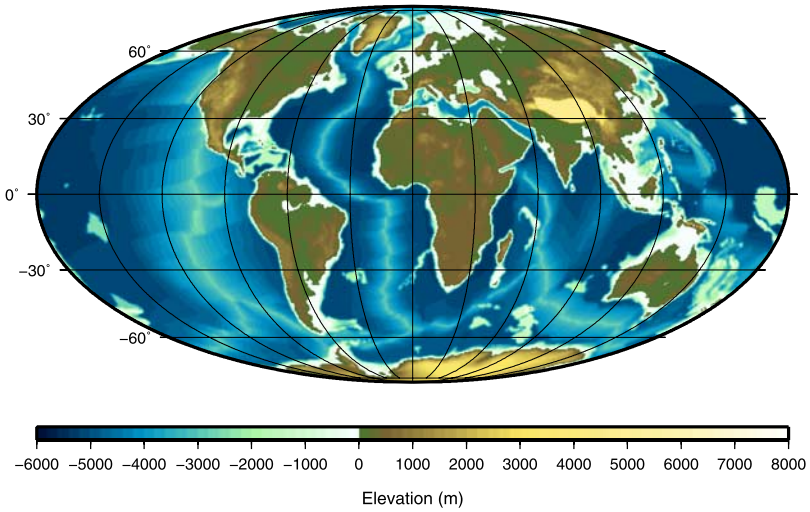

Figure 2. Present topography rotated to 15 Ma and merged with reconstructed paleobathymetry, with proxy-based adjustments to topography and geography (see text for details).

downsampled to a 2° × 2° resolution (Figure 3). All data sets were manipulated in the netCDF format.

2.2. Paleobathymetric Reconstruction

[7] Our middle Miocene paleobathymetry is constructed independent of our paleotopography and does not rely on the present-day bathymetry from ETOPO2. Instead, paleobathymetry is computed by converting age to depth using the GDH-1 age-depth relationship [*Stein and Stein*, 1992] using the paleoceanic age-area distribution of *Müller et al.* [2008b] and estimates of sediment accumulation, sediment loading and the eruption of large igneous provinces (LIPs). This approach was first applied by *Müller et al.* [2008b] to compute Cretaceous to present global bathymetry maps in 1 million year intervals for determining long-term sea level variations.

[8] Previous attempts to reconstruct paleobathymetry have mainly relied on the digital elevation models of the PALEOMAP project or on age-depth conversion constrained by *Müller et al.*'s [1997] present-day age grid [*Markwick and Valdes*, 2004]. We reconstruct the ocean basins using over 40,000 magnetic anomaly and fracture zone identifications, magnetic lineations, associated geological data, and the rotation model of *Müller et al.* [2008b] to create a set of seafloor-spreading isochrons from the Cretaceous to the present day. We reconstruct now subducted oceanic crust by addi-

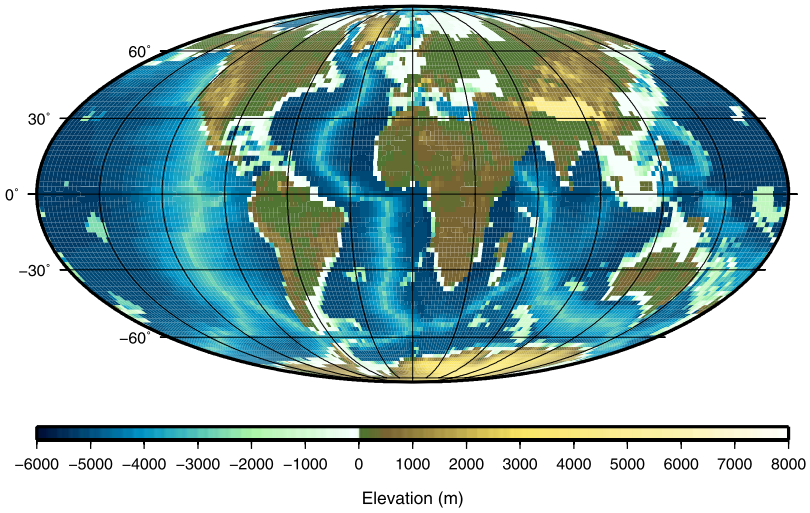

Figure 3. Present topography rotated to 15 Ma and merged with reconstructed paleobathymetry, with proxy-based and model-required adjustments to topography and geography, downsampled to 2° × 2° (see text for details).

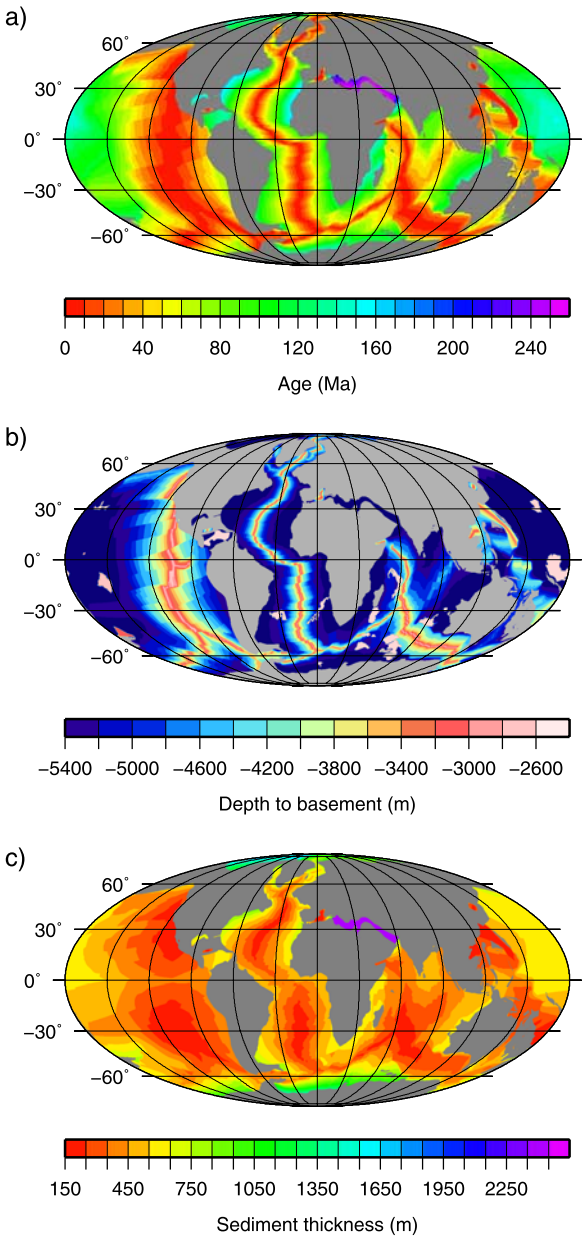

Figure 4. Reconstruction at 15 Ma showing the three major steps used to create the middle Miocene paleobathymetry (a) oceanic age model of *Müller et al.* [2008b], (b) depth to oceanic basement with oceanic large igneous provinces included using the age to depth calculation [*Stein and Stein*, 1992], and (c) estimated oceanic sediment thickness (see text for details). Grey areas correspond to nonoceanic lithosphere.

tionally using the rules of plate tectonics and onshore geological data to predict the geometry and lateral extent of ancient spreading ridge systems. We assume symmetrical spreading when reconstructing these "synthetic" isochrons. The data at 15 Ma is then extracted to create a global seafloor spreading isochron map for the middle Miocene and is the input for the age to oceanic basement depth conversion (Figure 4a).

[9] We tested four alternative age-depth relationships to find the best approximation for the thermal structure of the oceanic lithosphere; the plate boundary layer models of GDH-1 [*Stein and Stein*, 1992], *Crosby* [2007] and *Parsons and Sclater* [1977], and the thermal boundary layer model of *Crosby et al.* [2006]. Comparisons between the present-day residual basement and each age-depth model reveal that the GDH-1 [*Stein and Stein*, 1992] and *Crosby* [2007] plate models produced the best approximation of oceanic basement depth. The *Parsons and Sclater* [1977] relationship and thermal boundary layer models over-predict the depth of old ocean floor (see *Crosby et al.* [2006] for discussion). We apply the GDH-1 model [*Stein and Stein*, 1992] which produces relatively similar results to the *Crosby* [2007] plate model, to compute basement depth of the middle Miocene ocean floor (Figure 4b):

$$\text{If } t < 20 \text{ Ma}, \mathrm{d}(t) = 2600 + 365t^{1/2}$$

$$\text{If } t >= 20 \text{ Ma}, \mathrm{d}(t) = 5651 - 2473 \ \exp(-0.0278t)$$

where t is time in millions of years and d is depth in meters.

[10] Another component of paleobathymetric reconstructions is the eruption of LIPs on the ocean floor. The morphology of LIPs act as barriers in ocean circulation as they can be several kilometers higher than the surrounding ocean floor and have contributed 95–100 m to global sea level variations since the Cretaceous [*Miller et al.*, 2005; *Müller et al.*, 2008b]. We account for the eruption of LIPs in our paleobathymetry by using the LIP outlines and eruption ages of *Müller et al.* [2008b] and the method of *Schubert and Sandwell* [1989] to determine average LIP height above the surrounding ocean floor. The computed average height for each LIP is then added to the oceanic basement grids allowing for seafloor subsidence since LIP eruption.

[11] Changes in sediment thickness through time have been shown to be a function of oceanic crustal age and latitude due to variations in productivity between zones of tropical upwelling and an increase in sediment thickness toward high latitudes, reflecting terrestrial runoff (see *Davis and Elderfield* [2004] for details). We estimate oceanic sediment thickness for the middle Miocene (Figure 4c) by

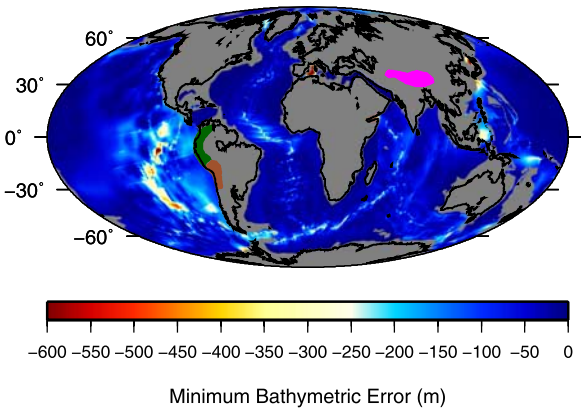

Figure 5. Uncertainty in Miocene bathymetry based on maximum age error reflecting the negative depth error (mean of −58 m). The positive depth error has the same spatial relationship but with a mean error of +66 m. The calculation of age uncertainties is detailed by *Müller et al.* [1997] and *Müller et al.* [2008b]. Highest errors correspond to areas of limited magnetic identification coverage (e.g., along the fast spreading East Pacific Rise, Central Atlantic, and several back-arc basins where magnetic identifications were not available). Areas of topographic uncertainty for the Tibetan Plateau shown by magenta polygon and Andean Cordillera shown by dark green and brown polygons; see Tables 1 and 2 for published error estimates.

fitting a polynomial surface linear in age and quadratic in latitude (i.e., five model parameters) as explained by *Müller et al.* [2008b]. The isostatic compensation of the predicted sediment thickness is calculated using the function from *Sykes* [1996]. In the middle Miocene, we predict a mean sediment thickness on ocean crust of approximately 270 m with an estimated error of ±15 m [*Müller et al.*, 2008b].

[12] Seafloor roughness is believed to have an effect on ocean circulation [e.g., *Polzin et al.*, 1997]. Our middle Miocene reconstruction shows a relatively smooth seafloor compared to the modern day as there is a lack of geological data to constrain seafloor roughness of now subducted oceanic crust. However, it may be possible to predict roughness based on seafloor spreading rate [*Malinverno*, 1991] and other parameters such as spreading obliquity and the thermal properties of the underlying mantle. The addition of an artificial seafloor roughness factor based on these parameters may be possible in future reconstructions.

[13] The unloaded sediments and LIPS are added to the depth-to-oceanic-basement prediction to produce a global middle Miocene paleobathymetric map (Figure 2). Paleobathymetric uncertainty is calculated by converting the maximum age error [*Müller et al.*, 2008b] into depth (Figure 5). Our paleobathymetry is downsampled to 2° × 2° to conform to our topography model (Figure 3). At each stage in the paleobathymetric reconstruction, latitudinal biasing is accounted for by assigning increasing aspect ratios when gridding with higher latitudes.

2.3. Model-Required Adjustments

[14] Adjustments are made to ensure that our reconstruction can be utilized as input into GCMs (Figure 3). Marginal seas are either removed (e.g., the Amazon) or connected to the global ocean (e.g., the Caspian and Black Seas). Isolated ocean grid cells can act as sources or sinks of residual surface energy flux in GCMs, which subsequently contribute to net energy imbalance at the model surface. Connection of marginal seas to the global ocean also ensures fresh water balance is maintained within oceanic grid cells without the need of a flux correction.

[15] Transport of fresh water from the continents to the oceans is not explicitly considered in our paleotopography. Areas of internal drainage such as intermontane basins and flat plateaus allow rivers to converge over land grid cells instead of flowing to the ocean. While these features exist in the reconstructed paleotopography, river runoff directions are calculated for models capable of treating river transport as an independent boundary condition (e.g., Community Land Model 3 [*Vertenstein et al.*, 2004]) and is available from the authors. River runoff directions are calculated based on the greatest slope between grid points. To avoid internal drainage, a boxcar filter with a width of 1200 km is applied to the paleotopography for these calculations, while the model input topography is left unfiltered. Although such a methodology is not suitable for many models, specifying river transport as an independent boundary condition allows topographic features to remain that would otherwise require smoothing or infilling.

[16] Seaways are widened to a minimum of two grid cells to ensure uninterrupted flow. This is required due to the staggering of variables in model grid space, where vector and scalar quantities are not located at the same point in a grid cell and result in oceanic grid cells adjacent to land having a zero velocity. For this purpose a grid cell size of 3.6° in longitude and 1.6° in latitude is assumed, approximately that of the coarse resolution Parallel

Table 1. Tibetan Plateau Paleoelevations

Location	Age (Ma)	Paleoelevation (m)	Error (m)	Latitude/ Longitude	References[a]
Dingqing Fm.	middle Miocene	4260	+475/−575	32°N/89.75°E	1
Niubao Fm.	middle Miocene	4850	+380/−460	32°N/89.75°E	1
Namling Basin	15	4689	±895	29.7°N/89.58°E	2
Namling Basin	15	4638	±847	29.7°N/89.58°E	2
Namling-Oiyug Basin	14–17	5200	+1370/−605	29.7°N/89.5°E	3
Gyirong Basin	after 7 Ma	<2900–3400	N.D.[b]	28.5°N/85.5°E	4

[a] References: 1, *Rowley and Currie* [2006]; 2, *Spicer et al.* [2003]; 3, *Currie et al.* [2005]; 4, *Wang et al.* [2006].
[b] N.D. is not determined.

Ocean Program version 2.0.1 (POP) [*Smith and Gent*, 2004]. For similar reasons, ocean depths are set to a minimum of three vertical levels (26 m, based on the POP). In some instances removal or combination of islands was necessary in widening seaways, particularly in South East Asia and North America (Figure 3). A significant adjustment is the closure of the narrow Tethys Seaway between Arabia and Africa. According to paleogeographical evidence [*Roegl*, 1999] initial closure of the Tethys seaway occurred during the Burdigalian, with intermittent connections during the middle Miocene and permanent closure by the late Miocene. As paleogeographic reconstructions represent a time average and adequate expansion of the seaway between Arabia and Africa would have been idealistic at best, it was regarded as satisfactory to close off the seaway completely (Figure 3). It is noteworthy however that an open Tethys seaway may have played a role in maintaining a warm middle Miocene climate [e.g., *Ramsay et al.*, 1998].

[17] Further adjustments to bathymetry are required for implementation into ocean GCMs but are not made here. Such adjustments are model and resolution dependent and significantly affect the majority of the bathymetry (e.g., degrading bathymetry to a models vertical resolution). To avoid removal of a potentially significant amount of detail, such adjustments are left to the end-user.

3. Middle Miocene Paleogeography and Paleotopography

[18] Following the rotation of continental plates to their middle Miocene positions (see section 2) modifications are applied to the paleogeography and paleotopography based on published geological data. Geological records are often both spatially and temporally limited. While a decrease in the time interval considered may increase the temporal precision of the data, this is often countered by a decrease in the density of available data points. In order to make our reconstruction as widely applicable as reasonable, quantitative paleoelevations from the Burdigalian to Langhian (approximately 20–14 Ma) are used to constrain the elevations of the Tibetan Plateau and Andean cordillera. These two mountain chains have particularly controversial uplift histories and a strong influence on climate [e.g., *Gregory-Wodzicki*, 2000; *Harris*, 2006]. Elevations from later periods of time which have implications for the early to middle Miocene are also included.

[19] Table 1 lists published quantitative paleoelevations for the Tibetan Plateau. The majority of evidence supports a near modern elevation of the southern and central plateau by the early to middle Miocene [*Coleman and Hodges*, 1995; *Currie et al.*, 2005; *Spicer et al.*, 2003; *Williams et al.*, 2001] or earlier [*Rowley and Currie*, 2006], with a minority maintaining that the main phase of uplift occurred during the late Miocene to Pliocene [*Wang et al.*, 2006; *Xu*, 1981; *Zhao and Morgan*, 1985]. On the basis of a wider variety of published paleoaltimetry methods and results, a maximum elevation of 4700 m is applied to the southern and central plateau. Elevation history of the northern plateau is not well constrained though speculations range from elevations of 3–4 km since the late Mesozoic [*Murphy et al.*, 1997], to rapid uplift since the Pliocene [*Harris*, 2006, and references therein]. We assume a relatively undeveloped northern plateau and reduce the northern extent of the whole plateau to reflect this. Elevation of the Indian plate prior to the India-Asia collision is also uncertain therefore a mean elevation of 100 m is applied to the area of the Indian plate that was subducted subsequent to 15 Ma (Figure 2).

Table 2. Andes Paleoelevations

Location	Age (Ma)	Paleoelevation (m)	Error[a] (m)	Latitude/ Longitude	References[b]
		Central Andes			
Potosi	13.8–20.8	2800	±2000	20°S/60°W	1
Atacama Desert	~15	1000–4500	N.D.[c]	24°S/69.5°W	2
Corocoro	middle Miocene	2000	±2000	17.5°S/68.7°W	3
Potosi	13.8–20.8	0–1320	±1200	20°S/60°W	4
Chucal	19–25	1000	±1500	18.8°S/69°W	5
Pislepampa	6–7	1200–1400	±1000	17.2°S/66°W	6
		Northern Andes			
Sal. de Tequendama II	middle Miocene	<700	±1500	6°N/74°W	7
Sal. de Tequendama I	early middle Miocene	<700	±1500	6°N/74°W	7
Sal. de Tequendama	middle Miocene	0–500	±1500	6°N/74°W	8

[a] Error calculated by *Gregory-Wodzicki* [2000], excluding reference 6.
[b] References: 1, *Berry* [1939]; 2, *Alpers and Brimhall* [1988]; 3, *Singewald and Berry* [1922]; 4, *Gregory-Wodzicki et al.* [1998]; 5, *Munoz and Charrier* [1996]; 6, *Graham et al.* [2001]; 7, *Wijninga* [1996]; 8, *Van der Hammen et al.* [1973].
[c] N.D. is not determined.

[20] Table 2 lists published quantitative paleoelevations for the Andes which were compiled and reviewed by *Gregory-Wodzicki* [2000], with an additional estimate from *Graham et al.* [2001]. Owing to the length of the cordillera and the north-south spread of data, southern, central, and northern sections are distinguished to encompass known elevations. Although no quantitative paleoelevations for the southern Andes were found, initiation of uplift in the southern Chilean Andes has been estimated to have occurred between 16 and 17.5 Ma [*Flynn et al.*, 2002]. *Malumian and Ramos* [1984] also infer maximum uplift of the southern Andes between 10 and 12 Ma, suggesting relatively low elevations before this time. Work on the central Andes from the early 20th century by *Berry* [1939] and *Singewald and Berry* [1922], as well as later work by *Alpers and Brimhall* [1988] suggest relatively high elevations during the middle Miocene (from *Gregory-Wodzicki* [2000]). More recent work examining paleofloras and crustal shortening however suggests that at least half of the mean modern elevation, approximately 3700 m, was achieved after 11 Ma [*Graham et al.*, 2001; *Gregory-Wodzicki et al.*, 1998]. Referring to the published data, a mean elevation of 600 m, 1000 m, and 500 m is applied to the southern, central and northern Andes, respectively.

[21] Some additional geographic and topographic adjustments are applied to our reconstruction. The opening of the Bering Strait has been dated between 4.8 and 7.4 Ma [*Marincovich and Gladenkov*, 1999]. Sediments found in Arctic waters containing Pacific Ocean diatoms, support earlier, intermittent openings (see *Sher* [1999] for discussion), though there are no precise age data and it is not known to what extent (vertically or horizontally) the strait may have been open, if at all, during the middle Miocene. We therefore close the Bering Strait.

[22] The Zagros Mountains are removed, since collision between the Eurasian and Arabian plates occurred between 20 and 10 Ma [*McQuarrie et al.*, 2003]. The opening of the Red Sea is related to the northward drift of the Arabian plate and occurred at approximately 25 Ma [*McQuarrie et al.*, 2003]; however, its areal extent during the middle Miocene is not clear and most likely existed at a subgrid scale. We therefore exclude the Red Sea from our reconstruction.

[23] In accordance with other paleogeographic reconstructions (PALEOMAP Project) [*Markwick*, 2007] the Hudson Bay is removed. The North American Rocky Mountains are reduced to 75% of their modern elevation and East African topography is reduced to approximately 25% of its modern elevation [*Ruddiman et al.*, 1997, and references therein].

[24] Global ice volume between 17 and 16 Ma is estimated between 25% and 70% of that of the present-day East Antarctic Ice Sheet [*Pekar and DeConto*, 2006]. Estimated Cenozoic surface profiles for Antarctica also imply a significantly reduced ice sheet during the early to middle Miocene [*Robin*, 1988]. Antarctic topography is reduced in our reconstruction by 1000 m; however, it is isostatically corrected by 718 m. While timing and extent of ice sheet formation on Greenland is

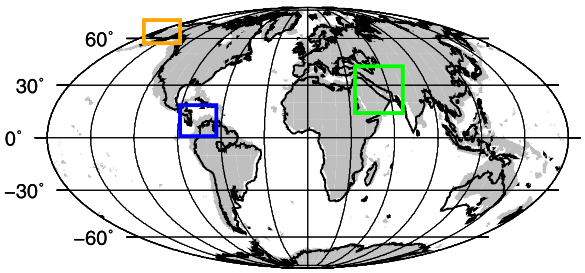

Figure 6. Coastlines for the Miocene (black line) and modern day (gray shade), colored squares show gateways which have opened or closed since the middle Miocene; Bering Strait (orange), Panama Strait (blue), and Tethys Seaway (green).

controversial [e.g., *Eldrett et al.*, 2007; *John and Krissek*, 2002; *Larsen*, 1994] it is assumed here that the warm climate of the early to middle Miocene [*Zachos et al.*, 2001] did not support significant ice sheets in the Northern Hemisphere. Greenland topography is therefore reduced by 2300 m and isostatically corrected by 1651 m.

[25] Sea level was also adjusted to represent middle Miocene conditions. On the basis of *Müller et al.* [2008b], we apply a 50 m sea level rise relative to the present, midway between the estimates of *Haq and Al-Qahtani* [2005] and *Miller et al.* [2005]. Further sea level rise applied to our paleotopography results in widespread continental flooding, which is not supported by geological observations and which would lead to a greater number of model corrections while not adding significant detail.

4. Discussion and Conclusion

[26] Our reconstructed tectonic boundary conditions are constrained by a combination of geological data, topographic and bathymetric assumptions, and general circulation modeling requirements. Uncertainties exist within these constraints and their climatic effect may be quantified in future climate sensitivity studies; however, we believe our reconstruction represents realistic middle Miocene surface conditions compliant with the requirements of GCMs.

[27] The geography of the middle Miocene and present are remarkably similar (Figure 6) and it may be argued that the resolution at which most paleoclimate experiments are performed is currently too coarse to resolve the differences. However, as computing power and standard operating resolutions increase these potentially significant differences may be resolved and will provide further avenues for investigating middle Miocene climate. Changes in idealized ocean gateway configurations from the Miocene to present have already been shown to significantly affect ocean circulation [*von der Heydt and Dijkstra*, 2006], demonstrating that geographic changes, in addition to other reconstructed boundary conditions, will be required to successfully simulate middle Miocene climate.

Acknowledgments

[28] Code by Samuel Levis and Christine Shields was used for the calculation of river transport directions. This work was carried out with funding from the Australian Research Council (ARC).

References

Alpers, C. N., and G. H. Brimhall (1988), Middle Miocene climatic change in the Atacama Desert, northern Chile: Evidence from supergene mineralization at La Escondida; with Suppl. Data 88–21, *Geol. Soc. Am. Bull.*, *100*(10), 1640–1656, doi:10.1130/0016-7606(1988)100<1640:MMCCIT>2.3.CO;2.

Berry, E. W. (1939), *The Fossil Flora of Potosi, Bolivia*, *Stud. in Geol.*, vol. 13, pp. 9–67, Johns Hopkins Univ. Press, Baltimore, Md.

Bice, K. L., et al. (2000), Quantifying the role of geographic change in Cenozoic ocean heat transport using uncoupled atmosphere and ocean models, *Palaeogeogr. Palaeoclimatol. Palaeoecol.*, *161*(3–4), 295–310, doi:10.1016/S0031-0182(00)00072-9.

Coleman, M., and K. Hodges (1995), Evidence for Tibetan plateau uplift before 14 Myr ago from a new minimum age for east-west extension, *Nature*, *374*(6517), 49–52, doi:10.1038/374049a0.

Crosby, A. G. (2007), Aspects of the relationship between depth and age on the Earth and Moon, Ph.D. thesis, 220 pp, Univ. of Cambridge, Cambridge, U. K.

Crosby, A. G., et al. (2006), The relationship between depth, age and gravity in the oceans, *Geophys. J. Int.*, *166*(2), 553–573, doi:10.1111/j.1365-246X.2006.03015.x.

Currie, B. S., et al. (2005), Middle Miocene paleoaltimetry of southern Tibet: Implications for the role of mantle thickening and delamination in the Himalayan orogen, *Geology*, *33*(3), 181–184, doi:10.1130/G21170.1.

Davis, E. E., and H. Elderfield (2004), *Hydrogeology of the Oceanic Lithosphere*, Cambridge Univ. Press, Cambridge, U. K.

Eldrett, J. S., et al. (2007), Continental ice in Greenland during the Eocene and Oligocene, *Nature*, *446*(7132), 176–179, doi:10.1038/nature05591.

Flynn, J. J., et al. (2002), A new fossil mammal assemblage from the southern Chilean Andes: Implications for geology, geochronology, and tectonics, *J. South Am. Earth Sci.*, *15*(3), 285–302, doi:10.1016/S0895-9811(02)00043-3.

Graham, A., K. M. Gregory-Wodzicki, and K. L. Wright (2001), Studies in neotropical paleobotany. XV. A Mio-Pliocene palynoflora from the Eastern Cordillera, Bolivia: Implications for the uplift history of the Central Andes, *Am. J. Bot.*, *88*(9), 1545–1557, doi:10.2307/3558398.

Gregory-Wodzicki, K. M. (2000), Uplift history of the Central and Northern Andes: A review, *Geol. Soc. Am. Bull.*, *112*(7), 1091–1105, doi:10.1130/0016-7606(2000)112<1091:UHOTCA>2.3.CO;2.

Gregory-Wodzicki, K. M., et al. (1998), Climatic and tectonic implications of the late Miocene Jakokkota flora, Bolivian Altiplano, *J. South Am. Earth Sci.*, *11*(6), 533–560, doi:10.1016/S0895-9811(98)00031-5.

Haq, B. U., and A. M. Al-Qahtani (2005), Phanerozoic cycles of sea-level change on the Arabian Platform, *GeoArabia*, *10*(2), 127–160.

Harris, N. (2006), The elevation history of the Tibetan Plateau and its implications for the Asian monsoon, *Palaeogeogr. Palaeoclimatol. Palaeoecol.*, *241*(1), 4–15, doi:10.1016/j.palaeo.2006.07.009.

John, K. E. K. S., and L. A. Krissek (2002), *The Late Miocene to Pleistocene Ice-Rafting History of Southeast Greenland*, pp. 28–35, Taylor and Francis, Philadelphia, Pa.

Larsen, H. C. (1994), Seven million years of glaciation in Greenland, *Science*, *264*(5161), 952–955, doi:10.1126/science.264.5161.952.

Malinverno, A. (1991), Inverse square-root dependence of mid-ocean-ridge flank roughness on spreading rate, *Nature*, *352*(6330), 58–60.

Malumian, N., and V. A. Ramos (1984), Magmatic intervals, transgression-regression cycles and oceanic events in the Cretaceous and Tertiary of southern South America, *Earth Planet. Sci. Lett.*, *67*(2), 228–237, doi:10.1016/0012-821X(84)90118-3.

Marincovich, L., and A. Y. Gladenkov (1999), Evidence for an early opening of the Bering Strait, *Nature*, *397*(6715), 149–151, doi:10.1038/16446.

Markwick, P. J. (2007), The palaeogeographic and palaeoclimatic significance of climate proxies for data-model comparisions, in *Deep-Time Perspectives on Climate Change: Marrying the Signal From Computer Models and Biological Proxies*, edited by M. Williams et al., pp. 251–312, Geol. Soc. of London, London.

Markwick, P. J., and P. J. Valdes (2004), Palaeo-digital elevation models for use as boundary conditions in coupled ocean-atmosphere GCM experiments: A Maastrichtian (late Cretaceous) example, *Palaeogeogr. Palaeoclimatol. Palaeoecol.*, *213*(1–2), 37–63.

McQuarrie, N., et al. (2003), Cenozoic evolution of Neotethys and implications for the causes of plate motions, *Geophys. Res. Lett.*, *30*(20), 2036, doi:10.1029/2003GL017992.

Miller, K. G., et al. (2005), The phanerozoic record of global sea-level change, *Science*, *310*(5752), 1293–1298, doi:10.1126/science.1116412.

Müller, R. D., et al. (1993), Revised plate motions relative to the hotspots from combined Atlantic and Indian Ocean hotspot tracks, *Geology*, *21*(3), 275–278, doi:10.1130/0091-7613(1993)021<0275:RPMRTT>2.3.CO;2.

Müller, R. D., et al. (1997), Digital isochrons of the world's ocean floor, *J. Geophys. Res.*, *102*(B2), 3211–3214, doi:10.1029/96JB01781.

Müller, R. D., et al. (2008a), Age, spreading rates and spreading asymmetry of the world's ocean crust, *Geochem. Geophys. Geosyst.*, *9*, Q04006, doi:10.1029/2007GC001743.

Müller, R. D., et al. (2008b), Long-term sea-level fluctuations driven by ocean basin dynamics, *Science*, *319*(5868), 1357–1362, doi:10.1126/science.1151540.

Munoz, N., and R. Charrier (1996), Uplift of the western border of the Altiplano on a west-vergent thrust system, Northern Chile, *J. S. Am. Earth Sci.*, *9*(3–4), 171–181, doi:10.1016/0895-9811(96)00004-1.

Murphy, M. A., et al. (1997), Did the Indo-Asian collision alone create the Tibetan Plateau?, *Geology*, *25*(8), 719–722, doi:10.1130/0091-7613(1997)025<0719:DTIACA>2.3.CO;2.

O'Neill, C., et al. (2005), On the uncertainties in hot spot reconstructions and the significance of moving hot spot reference frames, *Geochem. Geophys. Geosyst.*, *6*, Q04003, doi:10.1029/2004GC000784.

Parsons, B., and J. G. Sclater (1977), An analysis of the variation of ocean floor bathymetry and heat flow with age, *J. Geophys. Res.*, *82*(5), 803–827, doi:10.1029/JB082i005p00803.

Pekar, S. F., and R. M. DeConto (2006), High-resolution ice-volume estimates for the early Miocene: Evidence for a dynamic ice sheet in Antarctica, *Palaeogeogr. Palaeoclimatol. Palaeoecol.*, *231*(1–2), 101–109, doi:10.1016/j.palaeo.2005.07.027.

Polzin, K. L., et al. (1997), Spatial variability of turbulent mixing in the Abyssal Ocean, *Science*, *276*(5309), 93–96, doi:10.1126/science.276.5309.93.

Ramsay, A. T. S., et al. (1998), A model of early to middle Miocene deep ocean circulation for the Atlantic and Indian oceans, in *Geological Evolution of Ocean Basins: Results From the Ocean Drilling Program*, edited by A. Cramp et al., *Geol. Soc. London Spec. Publ.*, *131*, 55–70.

Robin, G. D. (1988), The Antarctic ice sheet; its history and response to sea level and climatic changes over the past 100 million years, *Palaeogeogr. Palaeoclimatol. Palaeoecol.*, *67*(1–2), 31–50, doi:10.1016/0031-0182(88)90121-6.

Roegl, F. (1999), Mediterranean and Paratethys: Facts and hypotheses of an Oligocene to Miocene paleogeography; short overview, *Geol. Carpathica*, *50*(4), 339–349.

Rowley, D. B., and B. S. Currie (2006), Palaeo-altimetry of the late Eocene to Miocene Lunpola basin, central Tibet, *Nature*, *439*, 677–681, doi:10.1038/nature04506.

Ruddiman, W. F., et al. (1997), Testing the climatic effects of orography and CO2 with General Circulation and Biome Models, in *Tectonic Uplift and Climate Change*, edited by W. F. Ruddiman, pp. 203–235, Plenum, New York.

Sandwell, D. T., and W. H. F. Smith (1997), Marine gravity anomaly from Geosat and ERS 1 satellite altimetry, *J. Geophys. Res.*, *102*(B5), 10,039–10,054, doi:10.1029/96JB03223.

Schubert, G., and D. Sandwell (1989), Crustal volumes of the continents and of oceanic and continental submarine plateaus, *Earth Planet. Sci. Lett.*, *92*(2), 234–246, doi:10.1016/0012-821X(89)90049-6.

Sewall, J. O., et al. (2007), Climate model boundary conditions for four Cretaceous time slices, *Clim. Past Discuss.*, *3*(3), 791–811.

Sher, A. (1999), Traffic lights at the Beringian crossroads, *Nature*, *397*(6715), 103–104, doi:10.1038/16341.

Singewald, J. T., and E. W. Berry (1922), *The Geology of the Corocoro Copper District of Bolivia*, *Stud. in Geol.*, vol. 1, pp. 1–117, Johns Hopkins Univ. Press, Baltimore, Md.

Smith, R., and P. Gent (2004), *Reference Manual for Parallel Ocean Program (POP)*, Los Alamos Natl. Lab., Los Alamos, N. M.

Spicer, R. A., et al. (2003), Constant elevation of southern Tibet over the past 15 million years, *Nature*, *421*(6923), 622–624, doi:10.1038/nature01356.

Stein, C. A., and S. Stein (1992), A model for the global variation in oceanic depth and heat flow with lithospheric age, *Nature*, *359*(6391), 123–129, doi:10.1038/359123a0.

Sykes, T. J. S. (1996), A correction for sediment load upon the ocean floor; uniform versus varying sediment density estima-

tions; implications for isostatic correction, *Mar. Geol.*, *133*(1–2), 35–49, doi:10.1016/0025-3227(96)00016-3.

Van der Hammen, T., et al. (1973), Palynological record of the upheaval of the northern Andes: A study of the Pliocene and lower Quaternary of the Colombian Eastern Cordillera and the early evolution of its high-Andean biota, *Rev. Palaeobot. Palynol.*, *16*(1–2), 1–42, doi:10.1016/0034-6667(73)90031-6.

Vertenstein, M., et al. (2004), *Community Land Model Version 3.0 (CLM3.0)*, *User's Guide*, Natl. Cent. for Atmos. Res, Boulder, Colo.

von der Heydt, A., and H. A. Dijkstra (2006), Effect of ocean gateways on the global ocean circulation in the late Oligocene and early Miocene, *Paleoceanography*, *21*, PA1011, doi:10.1029/2005PA001149.

Wang, Y., et al. (2006), Ancient diets indicate significant uplift of southern Tibet after ca. 7 Ma, *Geology*, *34*(4), 309–312, doi:10.1130/G22254.1.

Williams, H., et al. (2001), Age and composition of dikes in Southern Tibet: New constraints on the timing of east-west extension and its relationship to postcollisional volcanism, *Geology*, *29*(4), 339–342, doi:10.1130/0091-7613(2001)029<0339:AACODI>2.0.CO;2.

Wijninga, V. M. (1996), *Paleobotany and Palynology of Neogene Sediments From the High Plain of Bogota (Colombia)*, 370 pp., Univ. of Amsterdam, Amsterdam.

Xu, R. (1981), Vegetation changes in the past and the uplift of Qinghai–Xizang plateau, in *Geological and Ecological Studies of the Qinghai–Xizang Plateau*, vol. 1, pp. 139–144, Science Press, Beijing.

Zachos, J., et al. (2001), Trends, rhythms, and aberrations in global climate 65 Ma to present, *Science*, *292*(5517), 686–693, doi:10.1126/science.1059412.

Zhao, W.-L., and W. J. Morgan (1985), Uplift of Tibetan Plateau, *Tectonics*, *4*(4), 359–369, doi:10.1029/TC004i004p00359.